



Fermi National Accelerator Laboratory

FERMILAB-Conf-95/200-E

CDF

Proton-Antiproton Collider Physics

M.J. Shochet

*Fermi National Accelerator Laboratory
P.O. Box 500, Batavia, Illinois 60510*

*University of Chicago
Enrico Fermi Institute, Chicago, Illinois*

July 1995

Published Proceedings for the *10th Topical Workshop on Proton-Antiproton Collider Physics*,
Fermi National Accelerator Laboratory, Batavia, Illinois, May 9-13, 1995

Disclaimer

This report was prepared as an account of work sponsored by an agency of the United States Government. Neither the United States Government nor any agency thereof, nor any of their employees, makes any warranty, expressed or implied, or assumes any legal liability or responsibility for the accuracy, completeness, or usefulness of any information, apparatus, product, or process disclosed, or represents that its use would not infringe privately owned rights. Reference herein to any specific commercial product, process, or service by trade name, trademark, manufacturer, or otherwise, does not necessarily constitute or imply its endorsement, recommendation, or favoring by the United States Government or any agency thereof. The views and opinions of authors expressed herein do not necessarily state or reflect those of the United States Government or any agency thereof.

Proton-Antiproton Collider Physics

Melvyn J. Shochet

*Department of Physics and Enrico Fermi Institute
University of Chicago, Chicago, IL 60637*

Summary of the 10th $\bar{p}p$ Workshop, Fermilab, May 9-13, 1995.

I. INTRODUCTION

The 9th $\bar{p}p$ Workshop was held in Tsukuba, Japan in October, 1993 (1). A number of important issues remained after that meeting: Does QCD adequately describe the large cross section observed by CDF for γ production below 30 GeV? Do the CDF and D0 b -production cross sections agree? Will the Tevatron live up to its billing as a world-class b -physics facility? How small will the uncertainty in the W mass be? Is there anything beyond the Minimal Standard Model? And finally, where is the top quark? Presentations at this workshop addressed all of these issues. Most of them are now resolved, but new questions have arisen.

This summary focuses on the experimental results presented at the meeting by CDF and D0 physicists. Reviews of LEP and HERA results, future plans for hadron colliders and their experiments, as well as important theoretical presentations are summarized elsewhere in this volume. Section II reviews physics beyond the Minimal Standard Model. Issues in b and c physics are addressed in section III. Section IV focuses on the top quark. Electroweak physics is reviewed in section V, followed by QCD studies in section VI. Conclusions are drawn in section VII.

II. PHYSICS BEYOND THE MINIMAL STANDARD MODEL

At the Fermilab Tevatron, searches have been carried out for supersymmetric particles, additional high-mass gauge bosons, and other exotica.

A. Supersymmetry

There have been two major search modes for supersymmetric particles in $\bar{p}p$ collisions. The trilepton mode is sensitive to the production of chargino-neutralino pairs which decay into charged leptons plus the lightest supersymmetric particle (LSP), assumed to be a neutralino (2,3). The current chargino mass limit from the Tevatron is almost identical to the 45 GeV/ c^2 limit from LEP.

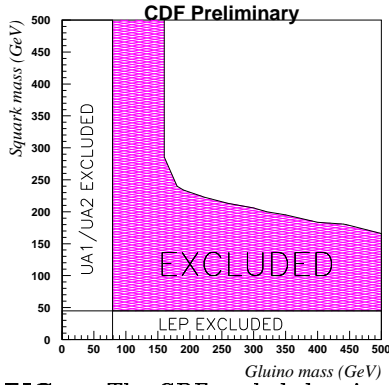


FIG. 1. The CDF excluded region in the squark-gluino mass plane for one possible set of SUSY parameters.

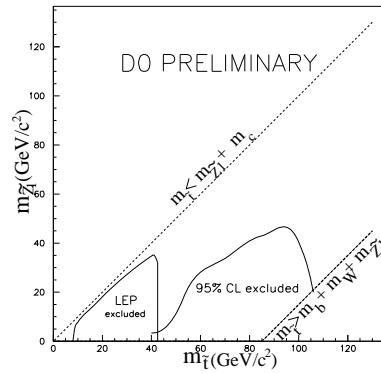


FIG. 2. The D0 excluded region in the stop-neutralino mass plane.

If squarks and gluinos are pair produced, they will decay to quarks and gluons plus LSPs. Hence the signature is multiple jets plus large missing E_T (\cancel{E}_T) from the undetected LSPs. For high mass squarks and gluinos, the modeling of the decay chain is complex because there is likely to be a multiparticle cascade through other neutralinos. The other difficulty in this search is the large Standard Model background from high P_T production of Z decaying into $\nu\bar{\nu}$ and W decaying into $l\nu$, where the lepton is either not observed or misidentified as a hadron jet. The minimum \cancel{E}_T requirement is set quite high in order to minimize these backgrounds. Similar limits on the squark and gluino masses were reported by CDF (2) and D0 (4). The excluded mass region from CDF is shown in Figure 1.

D0 has also searched for the top squark, which could be the lightest of the supersymmetric quarks (4). Since the predicted stop production cross section is an order of magnitude lower than the top production cross section, the stop would be more easily seen if its decay were not similar to that of the top quark. This would be the case if the stop quark were lighter than the charginos but heavier than the LSP neutralino, so that the dominant decay of the stop could be the neutral current $\tilde{t} \rightarrow c\tilde{Z}_1$. The resulting $\tilde{t}\tilde{t}$ signature is two acollinear jets plus large \cancel{E}_T . The D0 excluded mass region is shown in Figure 2.

B. New Gauge Bosons

Many extensions to the Minimal Standard Model have an extended gauge group and thus additional charged and neutral gauge bosons (W' , Z'). A peak in the dilepton mass distribution is the signature for a Z' (5,6). Figure 3 shows the CDF mass distributions. The absence of high mass events beyond those expected from γ/Z production results in the following lower limits on the Z' mass, assuming Standard Model couplings.

Dilepton mass distributions (CDF preliminary)

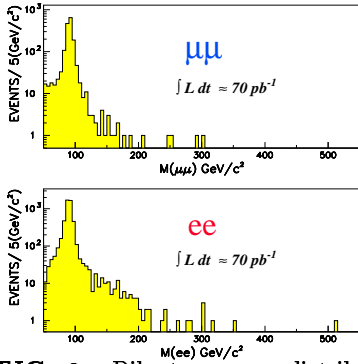
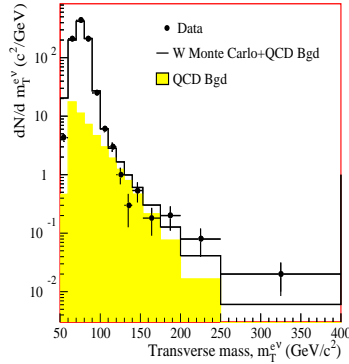


FIG. 3. Dilepton mass distributions from CDF.

FIG. 4. The D0 $e\nu$ transverse mass distribution.

$$M_{Z'} > 650 \text{ GeV}/c^2 \text{ @ 95\% CL} \quad (\text{CDF})$$

$$M_{Z'} > 480 \text{ GeV}/c^2 \text{ @ 95\% CL} \quad (\text{D0})$$

Most searches for a W' have assumed that the branching ratio to $e\nu$ and $\mu\nu$ is not greatly different than for the W . This can occur for a right-handed W' . The presence of such a W' would be seen as excess events with large $l\nu$ transverse mass. Figure 4 shows the $e\nu$ transverse mass distribution from D0.

The current mass limits for such a W' are

$$M_{W'} > 610 \text{ GeV}/c^2 \text{ @ 95\% CL} \quad (\text{D0})$$

$$M_{W'} > 652 \text{ GeV}/c^2 \text{ @ 95\% CL} \quad (\text{CDF})$$

If the decay $W' \rightarrow WZ$ is not suppressed, *e.g.* for a left-handed W' , then the branching ratio into WZ becomes 100% for high W' mass. CDF searched for this decay by looking for events with a high P_T electron, \cancel{E}_T , and two jets with a dijet mass near the Z mass. They exclude the region $205 < M_{W'} < 400 \text{ GeV}/c^2$.

D0 searched for the $e\nu_R$ decay of a right-handed W under the assumption that the right-handed neutrino is heavy and decays into an electron and a $q\bar{q}$ pair. For a relatively light ν_R , its decay products would overlap. In this case, they searched for a single high P_T electron plus jets. Cuts on E_T^e and the transverse mass were used to suppress the background from normal W production. If the ν_R were very heavy, the two electrons and two jets would generally be well separated. The mass limits from both search modes are shown in Figure 5.

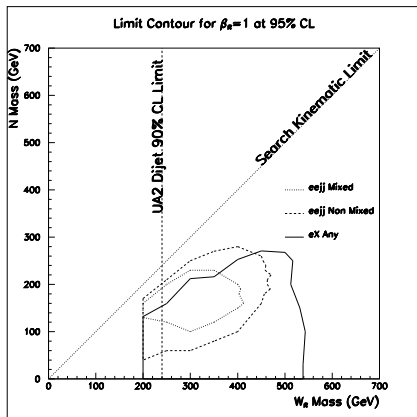


FIG. 5. The D0 excluded region in the $W_R - \nu_R$ mass plane for the single electron search and the two electron, two jet search.

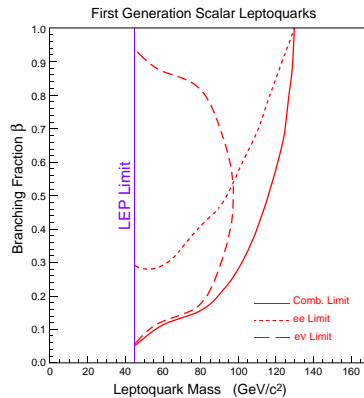


FIG. 6. The D0 limit on 1st generation leptoquarks.

C. Other Exotic Searches

The search for leptoquarks, which carry both lepton and baryon number, continues at the Tevatron. Unlike ep collisions, which could produce heavy first generation leptoquarks, high energy $\bar{p}p$ collisions could equally well produce any generation of leptoquarks. Thus far CDF and D0 have reported results on the search for first and second generation leptoquarks. Figure 6 shows the D0 limit for the first generation (3), while Fig. 7 gives the CDF result for the second generation (6).

CDF has searched for dijet resonances from sources such as axigluons, excited quarks, technirhos, diquarks, etc. (7) Figure 8 shows the difference between the data points and a smooth fit. Since there are no statistically significant deviations, CDF sets the limits shown in Fig. 9, which extend as high as 1 TeV in the case of axigluons. In an attempt to find objects with dominant coupling to third generation quarks, CDF has also looked at the dijet mass distribution when at least one of the jets is identified as a b -jet. Again no resonances are seen.

The D0 group reported on a search for a bosonic Higgs produced in association with a W or Z boson (3). The final state is $q\bar{q}\gamma\gamma$, with the $q\bar{q}$ coming from the vector boson and the photons from the Higgs. As shown in Fig. 10, the mass region $60 < M_H < 73.5 \text{ GeV}/c^2$ is excluded at the 90% confidence level.

At the Tevatron there is a very broad search for objects beyond the Minimal Standard Model. This will continue as a prime activity as long as the energy frontier remains at Fermilab.

FIG. 9. The excluded mass regions from the CDF dijet search.

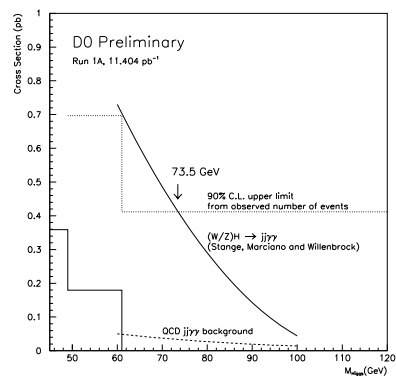


FIG. 10. The D0 upper limit on the bosonic-Higgs production cross section compared to the theoretical expectation.

III. B AND C QUARK PHYSICS

There are new and interesting results in two quite different areas. Production properties of b and c quarks address QCD issues, while studies of b decay test our understanding of the electroweak interaction.

A. Production

The basic question here is whether the standard next-to-leading-order QCD calculations adequately describe the production of heavy quarks. Of course before comparing data to theory, we must be sure that the experimental results are consistent.

In the past, heavy quark production cross sections were deduced from inclusive measurements. For single e or μ production, the contributions from b , c , and lepton misidentification had to be separated. The inclusive ψ and ψ' channels didn't suffer from the misidentification problem, but b production still had to be separated from $c\bar{c}$ production. In both cases, the momentum of the parent heavy quark had to be inferred from the daughter's momentum, which made the results dependent on the heavy quark fragmentation model.

With the CDF silicon vertex detector and large data samples, these problems have been greatly reduced by using exclusive and semi-exclusive final states. Figure 11 shows the size of the $B^\pm \rightarrow J/\psi K^\pm$ mass peak. There are also large samples of $B^0 \rightarrow J/\psi K^{*0}$ as well as $B \rightarrow \mu D^0 X$ and $B \rightarrow \mu D^{*\pm} X$ with the D or D^* fully reconstructed.

1. b Cross Section

A question that was initially raised at the last $\bar{p}p$ Workshop is whether the CDF and D0 b production cross sections agree. The latest D0 inclusive cross section (8,10) is shown in Fig. 12, while that for CDF (9) is shown in Fig. 13. Within the quoted uncertainties, the two data sets are in agreement.

CDF now presents a true differential cross section for B meson production using its exclusive and semi-exclusive data. Figure 14 shows that the measured cross section is still approximately a factor of 2 above the mean theoretical prediction.

Measuring the correlation between the b and \bar{b} quarks in an event can provide insight into the disagreement between the experimental and theoretical inclusive b cross sections. In addition, the correlations are needed for assessing the b -tag potential for CP violation and B_s mixing measurements. In Fig. 15, CDF dimuon data are used to obtain the $b\bar{b}$ production cross section as a function of the minimum P_T of the second b , given that the first b has P_T above 5 GeV/c. The data are consistent with the shape of the predicted cross section, but again the measured cross section is higher than expected.

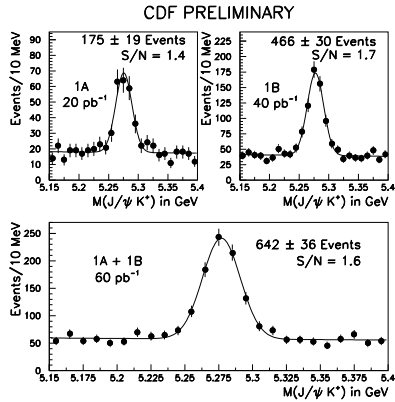


FIG. 11. The $B^\pm \rightarrow J/\psi K^\pm$ mass peak from CDF.

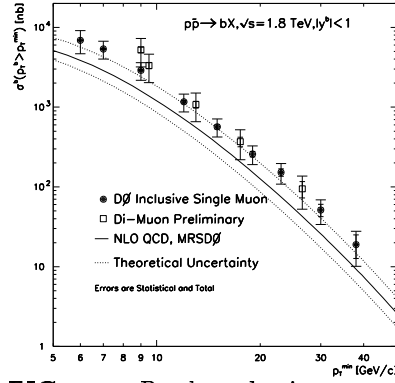


FIG. 12. D0 b -production cross section. Since each data point represents the integrated cross section above the plotted P_T , the uncertainties are correlated.

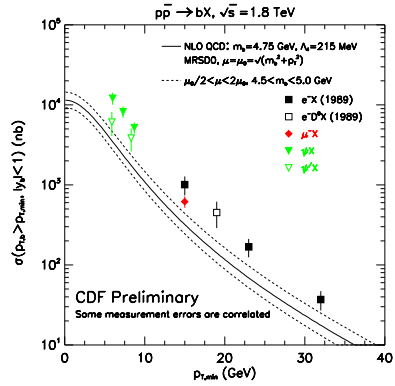


FIG. 13. CDF b -production cross section. Since each data point represents the integrated cross section above the plotted P_T , the uncertainties are correlated.

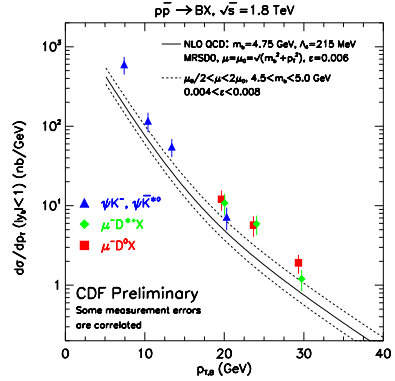


FIG. 14. B meson differential cross section from CDF compared to a NLO QCD calculation.

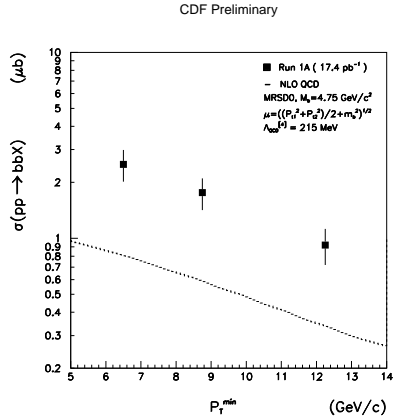


FIG. 15. CDF $b\bar{b}$ production cross section as a function of the minimum P_T of the second b , given that the first b has P_T above 5 GeV/c.

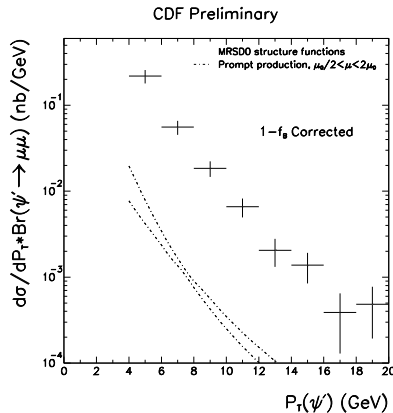


FIG. 16. The CDF cross section for promptly produced ψ' compared to the usual NLO QCD calculation.

2. Onia Production

Direct production of $c\bar{c}$ and $b\bar{b}$ bound states has replaced inclusive b production as the major outstanding issue in heavy quark production. CDF used its silicon vertex detector to separate prompt ψ and ψ' , produced at the primary $\bar{p}p$ vertex, from those coming from the decay of a B meson (11). Figure 16 shows the prompt ψ' cross section, which is more than an order of magnitude larger than that predicted from the usual NLO QCD calculations. The up-silon states, which are separately identified (Fig. 17), show a similar behavior (Fig. 18).

The surprisingly large direct production of onia led theorists to reconsider the production mechanisms. It was found by Braaten *et al*, Cacciari & Greco, Roy & Srinidhar, and others that diagrams not previously considered, like fragmentation of a gluon or a single heavy quark into an onium state, can be important. In a recent paper (12), Braatan & Fleming show that the addition of these color-octet fragmentation contributions give a cross section shape in agreement with the CDF data. However at present they are unable to calculate the absolute normalization of this additional contribution. Mangano (13) noted that at present the data are not being used to test theory, since complete theoretical calculations don't exist. Rather the Tevatron data on J/ψ , ψ' , χ , and Υ production provide the input needed to obtain a theoretical understanding of the process. Toward this end, additional experimental information is becoming available. CDF uses $\chi_C \rightarrow J/\psi + \gamma \rightarrow \mu^+\mu^- + e^+e^-$ to measure the production cross section for the individual χ states (Fig. 19). They find

$$\frac{\sigma_{\chi_{C2}}}{\sigma_{\chi_{C1}} + \sigma_{\chi_{C2}}} = 0.47 \pm 0.08 \pm 0.02$$

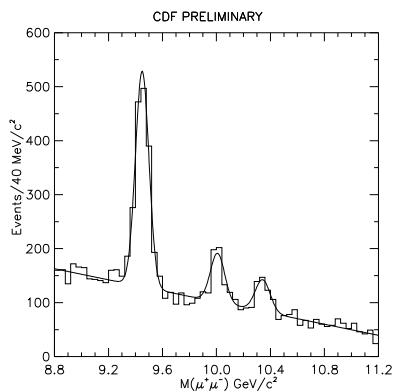


FIG. 17. CDF dimuon mass spectrum in the Υ region.

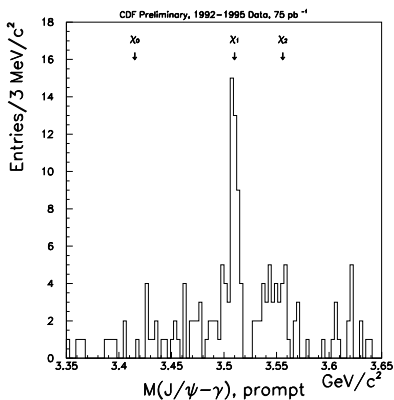


FIG. 19. CDF $J/\psi - \gamma$ mass spectrum in the χ region.

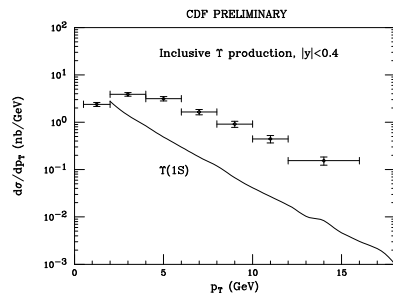


FIG. 18. The CDF $\Upsilon(1S)$ production cross section compared to a QCD calculation.

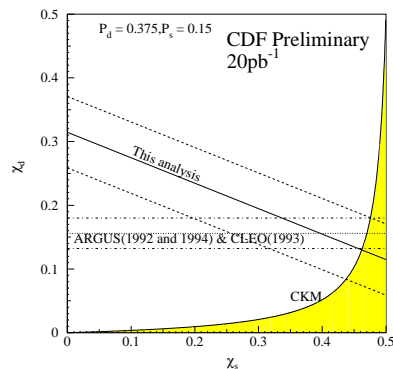


FIG. 20. CDF $\bar{\chi}$ result plotted in the χ_d, χ_s plane for assumed values of the relative B_d and B_s production rates.

In the near future, D0 will measure the J/ψ production cross section at large rapidity.

B. b Decay

The $\bar{p}p$ collider results on B decay are now having a major impact on the field. Results presented at the Workshop include $B - \bar{B}$ mixing and B meson lifetimes.

1. $B - \bar{B}$ Mixing

Until now, the $B - \bar{B}$ mixing results from $\bar{p}p$ colliders have been time integrated, using the ratio of the numbers of same sign to opposite sign dileptons.

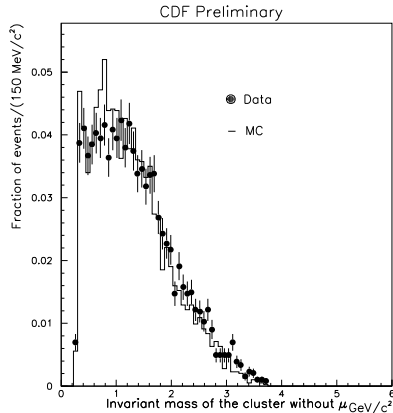


FIG. 21. Invariant mass of tracks pointing at the charm vertex in dimuon $b\bar{b}$ events.

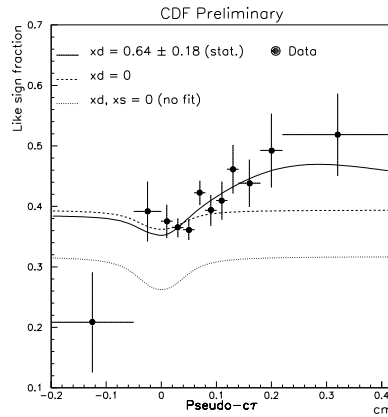


FIG. 22. The fraction of dimuons with the same electric charge as a function of the proper decay-time of one of the B mesons. The solid line is the best-fit mixing result.

This gives an average of B_d and B_s mixing weighted by the relative production rates of these mesons. The CDF result (14) (Fig. 20) for $e\mu$ events from the first 20 pb^{-1} of run I, $\bar{\chi} = 0.118 \pm 0.008 \pm 0.020$, has a statistical uncertainty that is smaller than for the LEP results. The D0 result (10) is $\bar{\chi} = 0.12 \pm 0.05 \pm 0.04$.

For the future, it is time-dependent $B - \bar{B}$ mixing, directly observing the $B - \bar{B}$ oscillations, that will be most important, for here the mixing parameters of B_d and B_s can be measured separately. The ratio, of course, provides a measurement of $|V_{td}/V_{ts}|$. The first task is to measure $x_d = \Delta m_d/\Gamma_d$, since the B_d oscillation period is relatively long. The future and much harder problem will be observing the very short B_s oscillation. In order to successfully carry out these measurements, excellent control of systematics is essential.

CDF measured the like-sign fraction of muon pairs from $b\bar{b}$ decay as a function of the proper lifetime of one of the B mesons (14). How well the vertex detector is understood can be seen in Fig. 21, which compares the measured invariant mass of the tracks pointing to the tertiary (charm) vertex with monte carlo simulation. The proper-time distribution of the like-sign fraction in μ pairs is shown in Fig. 22 along with the best-fit value for the mixing parameter, x_d . The result is $x_d = 0.64 \pm 0.18 \pm 0.21$ from the first 20 pb^{-1} of run I. With all the data now in hand, the overall uncertainty should be comparable to that from LEP.

2. B Lifetimes

Data from the Tevatron Collider are becoming dominant in the measurement of lifetimes of individual B mesons (14). Figure 23 shows the proper

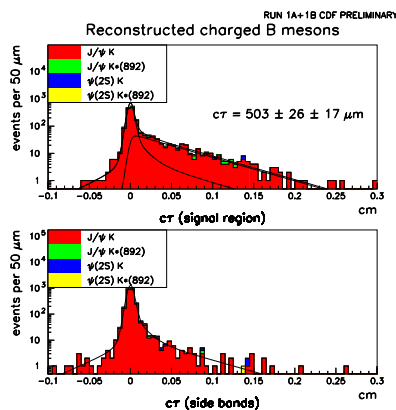


FIG. 23. The proper decay-time distribution for fully reconstructed B^\pm mesons. The lower plot shows the background shape from the mass sidebands.

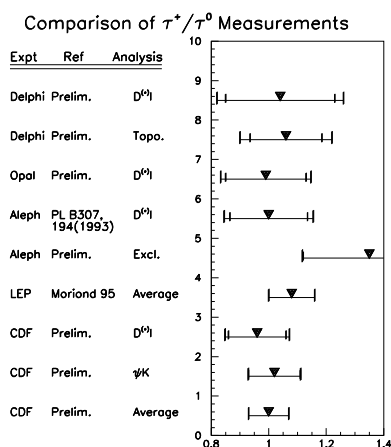


FIG. 24. Measured values of the ratio of the lifetimes for charged and neutral B mesons.

decay-time distribution for fully reconstructed B^\pm mesons. The CDF value for the ratio of the charged to neutral B meson lifetimes, $\tau^+/\tau^0 = 1.00 \pm 0.07$, is compared to other measurements in Fig. 24. If the full Tevatron run I integrated luminosity reaches 200 pb^{-1} , lifetime differences that are expected at the 5% level should be seen. In addition, if x_s is very large, the lifetime difference between the two CP eigenstates of the B_s might be observed.

3. Other B Decay Studies

There are a number of other studies currently in progress. For example, CDF has observed the Cabibbo suppressed decay $B^+ \rightarrow J/\psi \pi^+$ (Fig. 25). The ratio of the Cabibbo-suppressed to the Cabibbo-allowed branching ratios is

$$\frac{\text{BR}(B^+ \rightarrow J/\psi \pi^+)}{\text{BR}(B^+ \rightarrow J/\psi K^+)} = 4.9_{-1.7}^{+1.9} \pm 1.7\%$$

CDF has also searched for CP violation in B decay by looking for a difference between the numbers of $B\bar{B}$ events with a $\mu^+\mu^+$ pair and a $\mu^-\mu^-$ pair (14). The allowed regions from CDF and CLEO (15) are compared with the Standard Model prediction in Fig. 26.

B physics in pp collisions is still in its infancy. The CDF vertex detector expanded the opportunities enormously, and prospects for the rest of Tevatron run I and especially for run II are very bright. The ultimate reach of collider experiments will strongly depend on the efficiency with which B mesons can be flavor tagged. In this regard, Rosner (16) noted that LEP experiments have observed charge correlations between B mesons and nearby pions, while

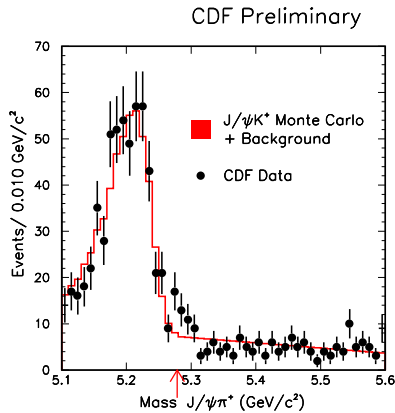


FIG. 25. The $J/\psi \pi$ mass plot showing the large background from $B \rightarrow J/\psi K$ and a small peak from $B \rightarrow J/\psi \pi$.

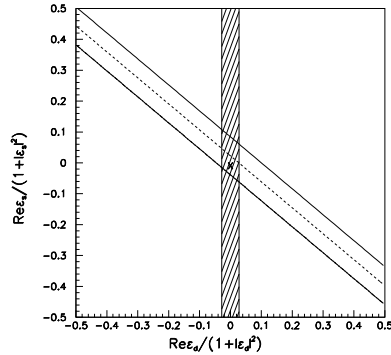


FIG. 26. The CDF (diagonal) and CLEO (vertical) allowed regions for the real part of the CP violation parameters ϵ_s and ϵ_d . CDF is sensitive to both because both B_d and B_s are produced at the Tevatron. The Standard Model prediction is the X near the point (0,0).

CDF has not yet reported a result. He suggested that the ability to flavor-tag using fragmentation hadrons could depend on the rapidity separation between the b and \bar{b} . This is large in Z^0 decay and variable in pp collisions. If this is a significant effect, then CDF should see a larger correlation in directly produced $b\bar{b}$ pairs than in gluon splitting into $b\bar{b}$.

IV. TOP QUARK

The most exciting hadron collider result of the past few years is of course the discovery of the top quark. At this Workshop, the evidence for the top quark was summarized, the mass calculations were presented, and the first kinematic and dynamic studies were shown.

A. Discovery

The first direct evidence for the top quark and the first measurement of its mass came from CDF in the spring of 1994 (17). With improved statistics, the top quark's existence was firmly established in the spring of 1995 by CDF (18) and D0 (19).

1. CDF

CDF found events consistent with $t\bar{t} \rightarrow WbW\bar{b}$ in two modes. Dilepton events (20) are produced when both W bosons decay leptonically (Fig. 27).

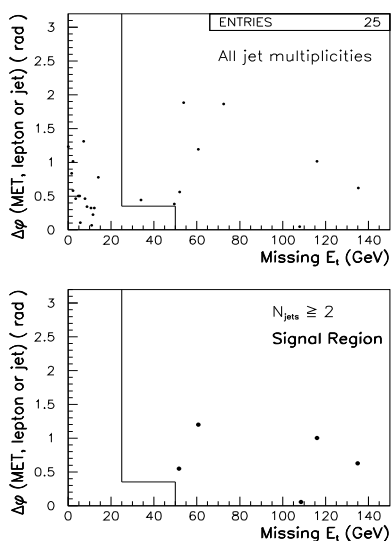


FIG. 27. The missing E_T vs. the azimuthal angle between the missing E_T vector and the nearest jet or lepton. Candidate top events contain at least 2 jets and are to the right of the solid curve.

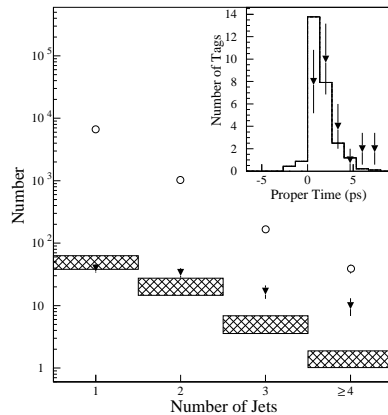


FIG. 28. The number of lepton+jet events (circles) as a function of the number of jets. The number of b -tagged jets (triangles) is compared to the calculated background (hatched regions). The inset shows the proper decay-time for tagged jets in events with 3 or more jets (data points) compared to that expected from b decay in top events (histogram).

Lepton+jet events (21) contain one W that decays leptonically, with the other decaying into a $q\bar{q}$ pair. CDF required 3 or more jets, at least one of which was identified as a b quark from either an observed secondary-decay vertex (Fig. 28) or an additional lepton from the b decay. From the excess number of events over expected background in all modes, CDF obtained the production cross section shown in Fig. 29.

CDF used lepton+jet events with at least 4 jets to reconstruct the top quark mass (22). Figure 30 shows the mass distribution for all events, without requiring that one jet be tagged as a b quark. A clear excess above background is seen in the $160 - 190 \text{ GeV}/c^2$ region. For events with a jet tagged as a b quark, the mass peak is very clear (Fig. 31), yielding $M_t = 176 \pm 8 \pm 10 \text{ GeV}/c^2$. For these events with an identified W boson decaying into leptons and one or two identified b -quark jets, CDF also found evidence for the W boson decaying into a jet pair. They released the dijet mass constraint in the fit and plotted the mass for the jet pair assigned to the W decay by the fitter. Figure 32 shows an excess over background in the W mass region.

2. $D0$

$D0$ also searched for the top quark in both the dilepton and lepton+jet channels (23). Figure 33 shows the scalar sum of the transverse energies of the

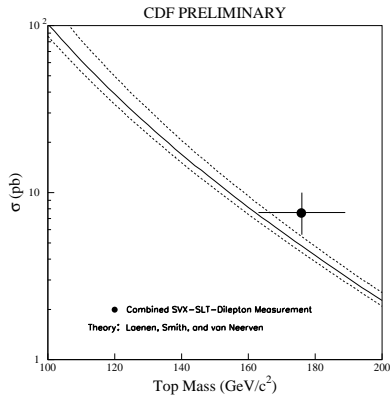


FIG. 29. The measured $t\bar{t}$ production cross section at CDF.

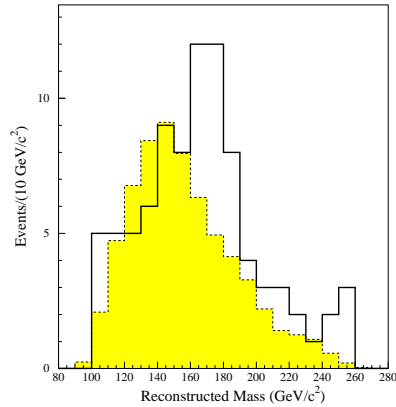


FIG. 30. The CDF reconstructed top-quark mass (solid histogram) for all events, without requiring that a jet be tagged as a b quark. The shaded region is the expected background shape.

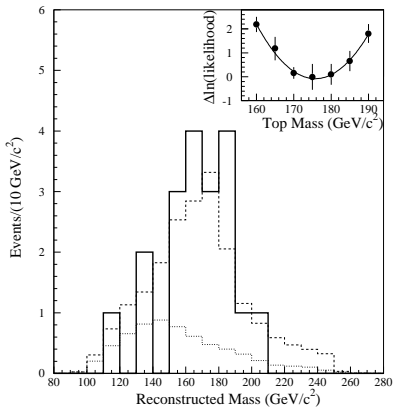


FIG. 31. CDF reconstructed top quark mass (solid) for events with a jet tagged as a b quark compared to the expected background (dotted) and to the expected signal plus background (dashed). The inset shows the results of the likelihood fit.

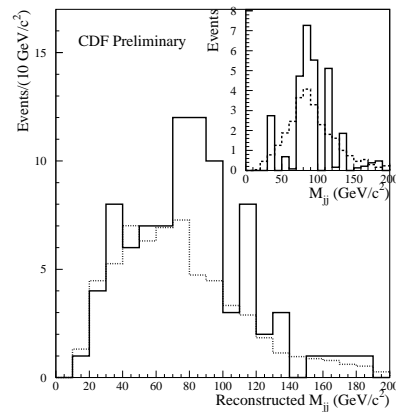


FIG. 32. The reconstructed di-jet mass (solid) for the pair of jets assigned to the W decay by the fitter. The distribution expected from non-top and combinatoric background is also shown (dotted). The excess is shown in the inset (solid), compared to the expected W distribution (dashed).

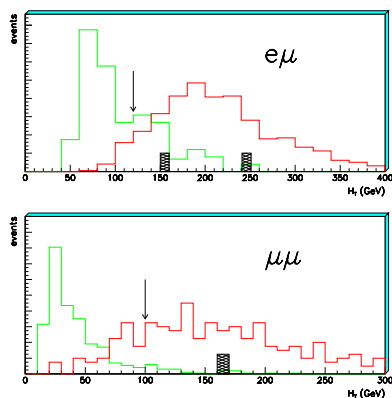


FIG. 33. The scalar sum of the transverse momenta of jets and electrons in the 3 D0 dilepton events. The dark and light histograms are the expectations for $t\bar{t}$ and background respectively.

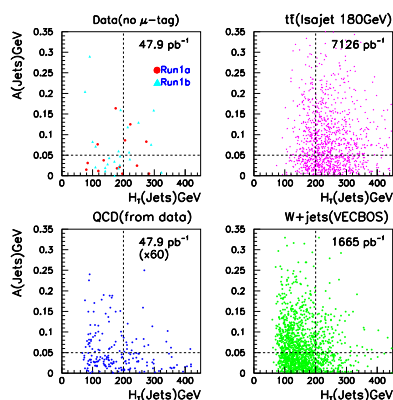


FIG. 34. The aplanarity vs. the sum of the jet transverse energies in D0 lepton+jet events containing at least 4 jets. Also shown are the distributions for backgrounds and from $t\bar{t}$ monte carlo.

jets and electrons in dilepton events. The observed events are in the region expected for $t\bar{t}$ events. In Fig. 34, the aplanarity vs. the total transverse energy of the jets is shown for lepton+jet events with at least 4 jets. The region above and to the right of the dotted lines is the signal region. The production cross section is compared with theory in Fig. 35. D0 got a similar cross section using a multivariate analysis (24).

D0 also did a constrained fit to lepton+jet events containing at least 4 jets (Fig. 36) (25). Their standard event selection cuts gave a purer signal sample, but they found a smaller statistical uncertainty using a looser set of cuts, giving $M_t = 199^{+19}_{-21} \pm 22 \text{ GeV}/c^2$. They also found evidence for a dijet mass peak near the W mass. Figure 37 shows the dijet mass distribution for

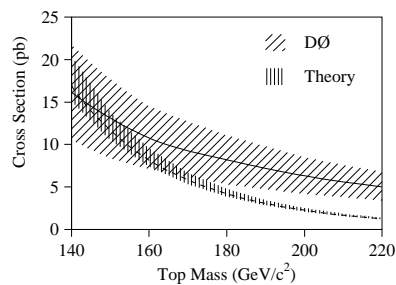


FIG. 35. The $t\bar{t}$ production cross section from D0. The top mass dependence is due to the detector acceptance.

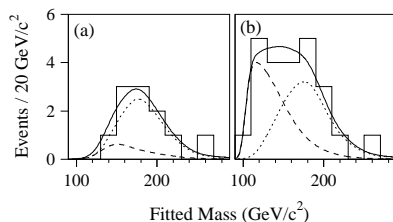


FIG. 36. Reconstructed top-quark mass in D0 lepton+jet events with at least 4 jets for (a) standard cuts and (b) loose cuts. The dotted and dashed curves are the signal and background shapes; the solid curve is the sum.

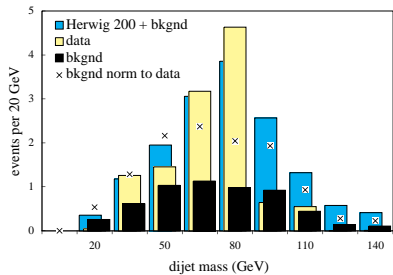


FIG. 37. The D0 dijet mass distribution for $t\bar{t}$ candidates with reconstructed top quark mass above $150 \text{ GeV}/c^2$.

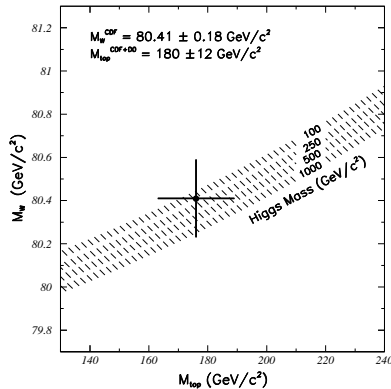


FIG. 38. The measured masses of the top quark and the W boson compared to Standard Model calculations for a variety of Higgs masses.

$t\bar{t}$ candidates with reconstructed top quark mass above $150 \text{ GeV}/c^2$.

B. Properties of the Top Quark

Now that the top quark has been discovered, the focus shifts to studying its properties. This critically depends on the size of the data sample. Thus the highest priority is to collect more data, *i.e.* keep the Collider running!

The most important characteristic of the top quark is its mass (Fig. 38). Together with the CDF measurement of the W mass, it provides an important test of the Standard Model. Additional data are needed to reduce both the statistical uncertainty and the systematic uncertainty in deducing the quark momentum from the energy of a calorimeter cluster. The latter can be controlled both by measuring the dijet mass peak in top events and by using a variety of control samples.

One way to study the top-quark decay vertex is to measure top branching ratios. CDF made the first such measurement using the numbers of top candidate events with one or two jets tagged as b quarks (26). They found

$$\frac{\text{BR}(t \rightarrow Wb)}{\text{BR}(t \rightarrow Wq)} = 0.87^{+0.13+0.13}_{-0.30-0.11}$$

Other studies of the decay vertex, such as decay angular distributions, are just beginning.

Studying the $t\bar{t}$ production vertex is largely a search for non-standard production mechanisms. The measured production cross section is consistent with the most recent theoretical calculation (Fig. 39) (27). To search for resonance production of $t\bar{t}$, CDF looked at both the net transverse momentum (Fig. 40) and invariant mass (Fig. 41) of the $t\bar{t}$ pair.

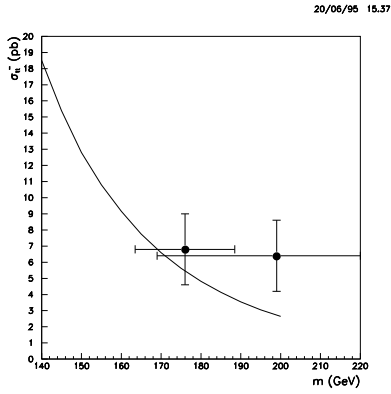


FIG. 39. The measured $t\bar{t}$ production cross section compared to the latest theoretical calculation. The CDF (D0) data point is on the left (right).

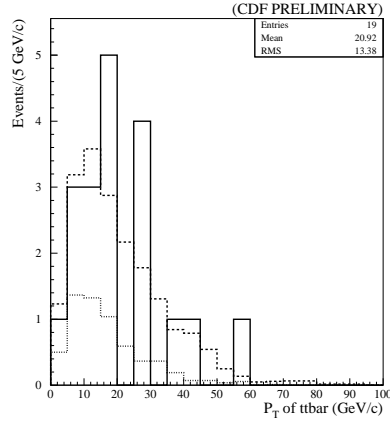


FIG. 40. The P_T of the $t\bar{t}$ pair from CDF (solid) compared to the background (dotted) and expected $t\bar{t}$ +background (dashed).

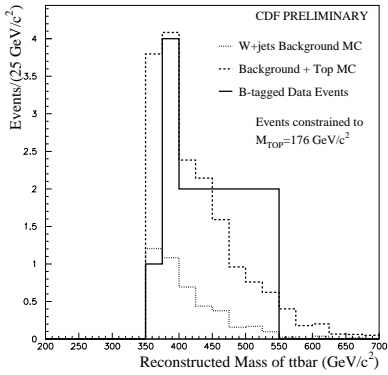


FIG. 41. The invariant mass of the $t\bar{t}$ pair from CDF (solid) compared to the background (dotted) and $t\bar{t}$ +background (dashed).

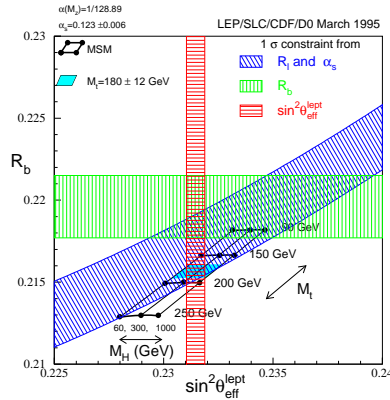


FIG. 42. Results from Z^0 decay compared with the top mass measurements and Standard Model predictions.

The excitement of discovery now changes to the exciting *possibility* that this very heavy state will reveal some of Nature's hidden secrets. Although much of the focus of this work is at the Tevatron Collider, it is a world-wide effort. Figure 42 compares Z-decay measurements, the top mass measurement, and Standard Model predictions (28). Except for the R_b measurement, which lies less than 2σ high, the data and the prediction agree well.

V. ELECTROWEAK PHYSICS

There were reports at the Workshop on a number of electroweak analyses. Results on vector boson production and decay provide an indirect measure of the W boson lifetime. The W mass has been measured a factor of two more precisely than before. Vector-boson pair production has been investigated in a variety of channels.

A. Vector Boson Production and Decay

The most precise measurement of the lifetime of the W comes from the ratio of W and Z production cross sections times branching ratio into leptons, $R \equiv \sigma B(W \rightarrow l\nu)/\sigma B(Z \rightarrow l^+l^-)$ (29). The W lifetime is extracted using the Z lifetime and partial width into leptons measured at LEP, the calculated ratio of the W to Z production cross sections, and the Standard Model calculation for the W partial width into leptons. The precision continues to improve as the vector boson data sample at the Tevatron grows (Fig. 43). The results from the first 10-20 pb^{-1} of run I are $R = 10.90 \pm 0.32 \pm 0.29$ (CDF) and $R = 10.90 \pm 0.49$ (D0), which translate into $\Gamma(W) = 2.064 \pm 0.061 \pm 0.059$ GeV (CDF) and $\Gamma(W) = 2.044 \pm 0.092$ GeV (D0). These agree well with the expectation in the Minimal Standard Model, $\Gamma(W) = 2.077 \pm 0.014$ GeV. When a few fb^{-1} of data are collected, the best measurement of $\Gamma(W)$ will come directly from the shape of the $W \rightarrow l\nu$ transverse mass distribution (30).

The mass distribution of lepton pairs (l^+l^-) can be used to measure parton distribution functions at low x and the Z production cross section, and to search for exotic objects, such as quark compositeness or heavy Z bosons. A preliminary mass distribution from CDF agrees with a leading order theoretical calculation (Fig. 44) (31).

B. W Decay

The precise value of the W mass is key to testing the Standard Model. CDF has submitted to PRL and PRD its final result from Tevatron run Ia (32). In order to achieve an overall uncertainty approaching 0.2%, they needed extraordinary control of systematics. The momentum scale of their spectrometer was confirmed with a large sample of $J/\psi \rightarrow \mu^+\mu^-$ events (Fig. 45) that produced a J/ψ mass measurement to $2 \text{ MeV}/c^2$. The Υ and Z masses provided

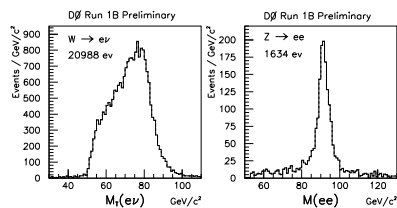


FIG. 43. The D0 $W \rightarrow e\nu$ and $Z \rightarrow e^+e^-$ samples for 25 pb^{-1} .

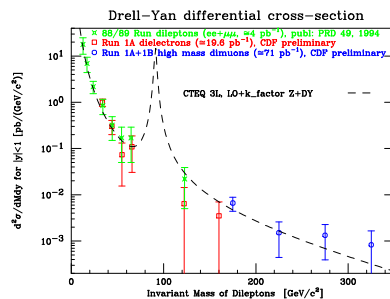


FIG. 44. The CDF lepton-pair production cross section compared to a leading order theoretical calculation.

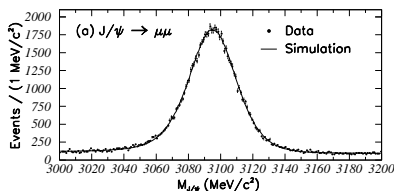


FIG. 45. CDF dimuon spectrum in the J/ψ region compared to a full simulation.

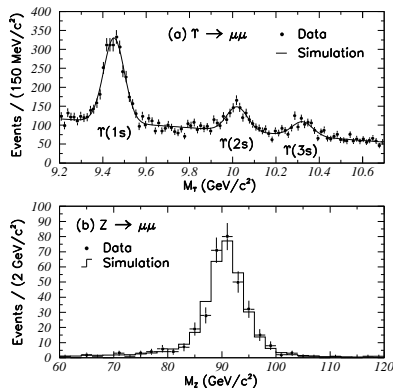


FIG. 46. CDF dimuon spectra in the (a) Υ and (b) Z regions.

further checks (Fig. 46). The ratio of the energy deposited in the calorimeter to the momentum measured in the tracking chamber for electrons from W decay provided a number of checks (Fig. 47). The location of the peak at 1.0 confirmed the energy scale of the electromagnetic calorimeter, while the shape and size of the high-side tail checked the amount of material between the beamline and the tracking chamber as well as the detailed modeling of electron bremsstrahlung.

The W mass was determined from fits to the $l\nu$ transverse mass spectra (Fig. 48). The result, $M_W = 80.410 \pm 0.180 \text{ GeV}/c^2$, has a factor of two smaller uncertainty than any previous result. Figure 49 shows that this mass is consistent with the predictions of the Standard Model.

A major systematic uncertainty in measuring the W mass is knowledge of the parton distribution functions within the proton. Most important is the difference between the up-quark and down-quark functions, since this affects the longitudinal momentum of the W and, through detector acceptance, the shape of the transverse mass distribution. Fortunately, the u/d ratio can be

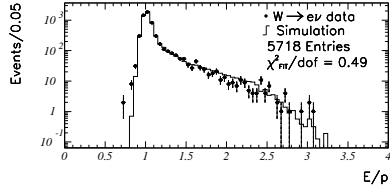


FIG. 47. Calorimeter energy divided by tracking momentum for electrons from W decay compared to a simulation with radiative effects included.

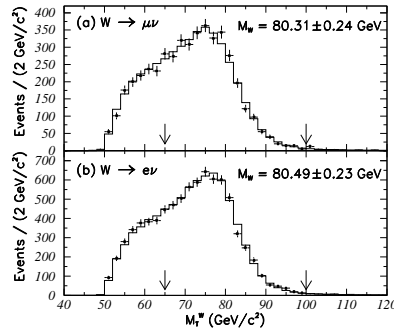


FIG. 48. Transverse mass distributions for CDF (a) $W \rightarrow \mu\nu$ and (b) $W \rightarrow e\nu$ events. The fit regions are delimited by arrows.

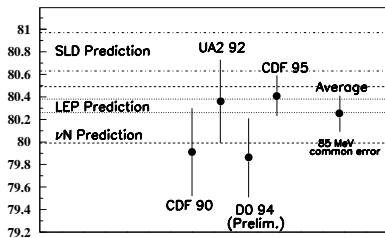


FIG. 49. Recent W mass results along with Standard Model predictions from neutrino cross sections (dashed), LEP data (dotted), and SLD data (dot-dashed).

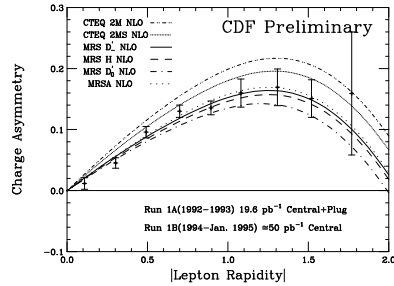


FIG. 50. CDF lepton charge asymmetry vs. the magnitude of the lepton rapidity. The curves are for various sets of parton distribution functions.

measured in the relevant x and q^2 region using the “W asymmetry”, the lepton charge asymmetry in W decay, as a function of the rapidity of the lepton (31). Figure 50 shows how this data limits the allowed parton distribution functions.

C. Diboson Production

Triboson couplings are essential in the Standard Model to cancel divergences that would otherwise appear in such processes as $q\bar{q} \rightarrow W^+W^-$. The diagram with a neutral vector boson in the s channel destructively interferes with the diagram in which a quark is exchanged in the t channel. At hadron colliders, the strength of the triboson couplings are studied in two channels: the production of photons in events containing a W or Z boson, and the production of a pair of heavy vector bosons.

1. $W\gamma$ and $Z\gamma$ Production

The first characteristic to check is the overall production rate (33). The measured cross sections for producing an energetic photon with a W is 21 ± 3 pb (CDF) and 15 ± 5 pb (D0), which are consistent with the Standard Model prediction of 18.5 ± 3 pb. For the production of $Z + \gamma$, CDF measures 5.7 ± 1.4 pb vs. the Standard Model value of 4.8 ± 0.5 pb.

A method more sensitive to anomalous triboson couplings is the study of the kinematics of the produced γ . Figure 51 shows the P_T of the γ compared to expectations. An anomalous coupling would appear as an excess at large P_T . CDF and D0 are able to place limits on the CP conserving anomalous $WW\gamma$ couplings as shown in Fig. 52. One effect of the interference of diagrams in the Standard Model is a dip in the photon angular distribution near $\cos \theta^* = 0.3$. The first data from CDF looking for this radiation zero are shown in Fig. 53. This is a clear case where more data is desperately needed.

2. WW and WZ Production

The triboson couplings at a WWZ vertex can be studied by looking for events containing two W bosons or a W and a Z (34). Upper limits on diboson production have come from looking for leptonic-hadronic decays, where one vector boson decays into $l\nu$ and the other into a $q\bar{q}$ pair. To minimize the background from the production of a single W or Z plus multiple jets, the search requires that the vector bosons be produced with large P_T . The absence of a diboson signal translates into the limits on anomalous couplings shown in Fig. 54.

The other possibility is to search for WW events in which both W's decay into leptons. To suppress background from $t\bar{t}$ decay, an event is required to contain no jets. D0 has one candidate event, from which they derive an upper limit of $\sigma(\bar{p}p \rightarrow WWX) < 87$ pb at the 95% confidence level. CDF sees 5 events. The \cancel{E}_T distribution is compared to a WW monte carlo calculation in

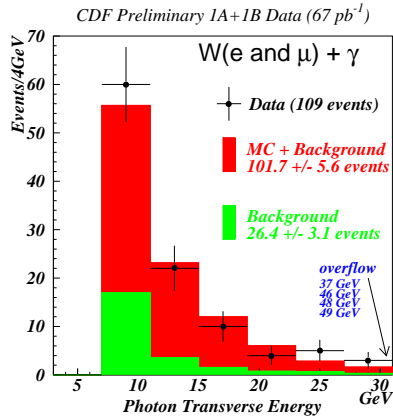


FIG. 51. The γE_T distribution in W events compared to the expectation from Standard Model production plus background.

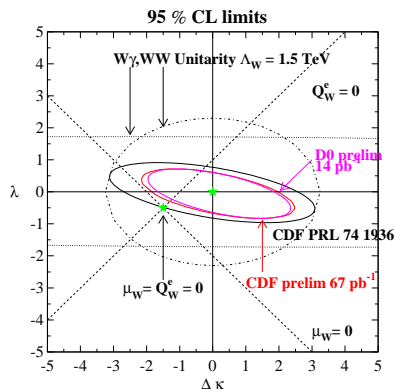


FIG. 52. The CDF and D0 limits on the anomalous $WW\gamma$ couplings $\Delta\kappa$ and λ .

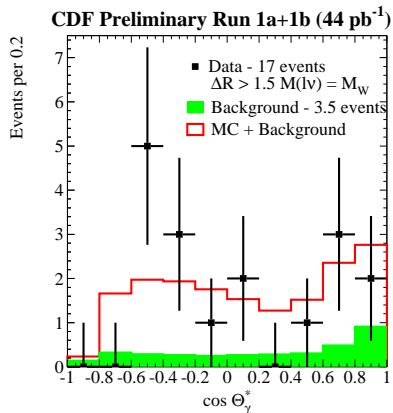


FIG. 53. The CDF photon angular distribution in the $W\gamma$ rest frame compared to the predicted dip near $\cos \theta^* = 0.3$.

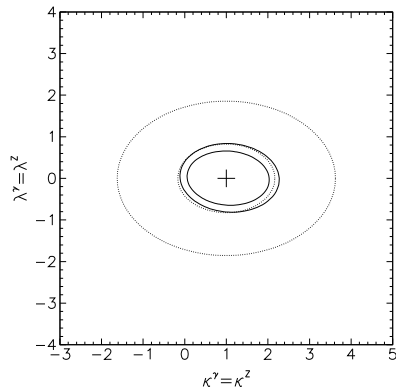


FIG. 54. Limits from CDF on anomalous WWZ couplings. The solid lines are the experimental limits; the dotted lines are the unitarity bounds. For each pair, the inner (outer) curve is for a form-factor scale of 1.5 TeV (1 TeV).

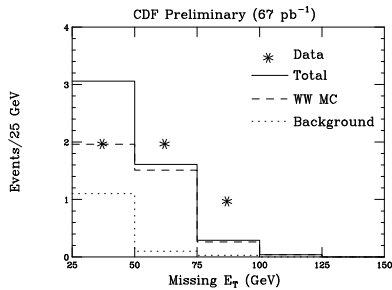


FIG. 55. The missing E_T in CDF WW candidate events compared to expectation from the Standard Model plus background.

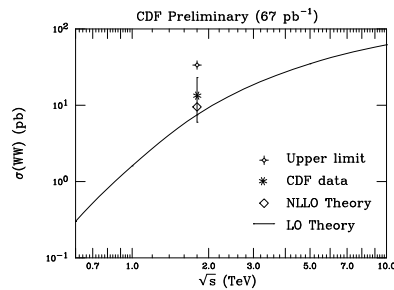


FIG. 56. The measured WW production cross section from CDF compared to the Standard Model prediction.

Fig. 55. Their measured cross section, $\sigma(\bar{p}p \rightarrow WWX) = 13.8^{+9.2}_{-7.4} \pm 2.9$ pb, is compared to theory in Fig. 56.

VI. QCD STUDIES

The strong interaction can be studied in a wide variety of channels in $\bar{p}p$ collisions. At the Workshop, results were presented on jet production, vector boson production, and hard diffraction and rapidity gaps.

Walter Giele noted that high statistics samples of jets, photons, W bosons, and Z bosons could yield a precision measure of α_s and most of the parton distribution functions all in a single experiment (35). As an example, he showed his extraction of α_s as a function of E_T from CDF inclusive jet-production cross sections from the 1988-89 data run (Fig. 57). Even from this relatively small data sample, the running of α_s is clearly seen, and the uncertainty in $\alpha_s(M_Z)$ is comparable to the best other determinations of the coupling constant.

A. Jet Production

1. Inclusive Jet Cross Section

With the large data sets collected at the Fermilab Collider, CDF and D0 have measured jet cross sections to $E_T = 450$ GeV, half way to the kinematic limit (36). D0 results for two rapidity regions are shown in Fig. 58. The data lie somewhat above the prediction, but the experimental systematic uncertainty is large enough to cover this difference.

The CDF cross section is shown in Fig. 59. On this 11 decade plot, the agreement with theory looks reasonably good. However, a linear plot (Fig. 60) shows that whereas agreement between data and theory is excellent below 200 GeV, the data slopes away from the prediction above that E_T . As presently

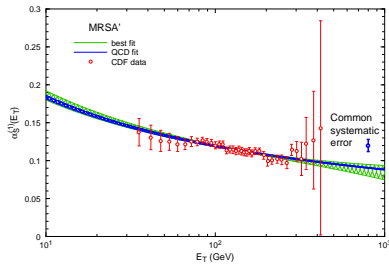


FIG. 57. Values for α_s , determined by Giele from CDF inclusive jet production cross sections and NLO QCD.

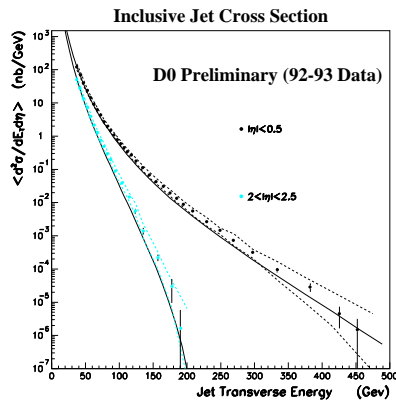


FIG. 58. D0 inclusive jet production cross section vs. E_T for two rapidity regions. Systematic uncertainties are shown by the dotted lines. The solid curves are QCD calculations.

understood, the correlated systematic uncertainty doesn't allow for such a break in the slope. CDF is currently studying all sources of systematics that could alter the cross section at large E_T . If this study does not turn up an experimental explanation, then either the next-to-leading-order QCD calculation is wrong, or there is new physics here.

2. Dijet Production

CDF has looked at two-jet data to gain insight into the excess observed in the inclusive spectrum. They see the excess for any rapidity of the second jet (Fig. 61) and in the dijet invariant mass distribution (Fig. 62).

D0 has used dijet events to measure the triple-differential cross section, which is sensitive to the gluon distribution function in the proton (37). Figure 63 compares the measured cross section vs jet rapidity with a QCD calculation. D0 finds that some parton distribution functions agree with the data at small η , while others agree at large η . However none is a good match over the entire rapidity range.

3. Multijets

Multijet production cross sections can be used to test rather complex QCD calculations (38). Understanding these processes is important, since they are background in many searches for physics beyond the Standard Model. Figure 64 shows the jet P_T distribution for events with large total E_T and 2-6 jets. The data are compared with both leading-order QCD calculations

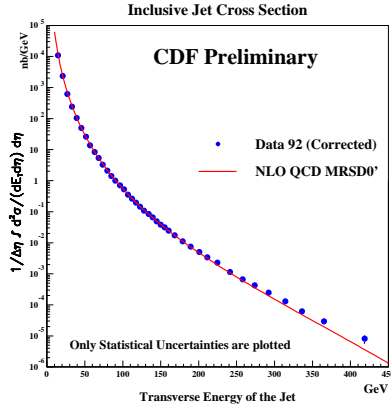


FIG. 59. The CDF inclusive jet production cross section compared to a NLO QCD calculation.

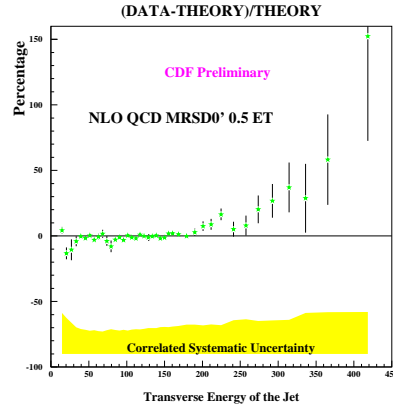


FIG. 60. The percentage difference between the CDF inclusive jet cross section and theory.

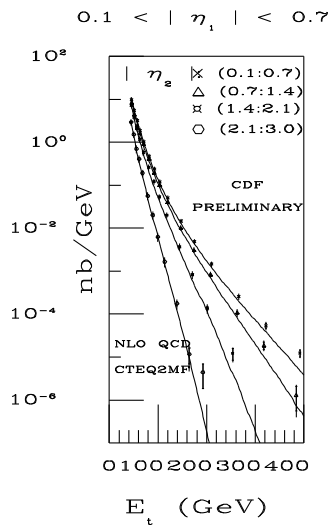


FIG. 61. CDF jet cross section vs E_T for different rapidity regions for the second jet in the event.

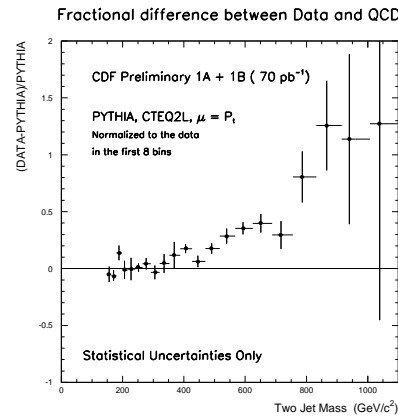


FIG. 62. The fractional difference between the CDF dijet mass distribution and the theoretical prediction. The theory is normalized to the data in the first 8 bins.

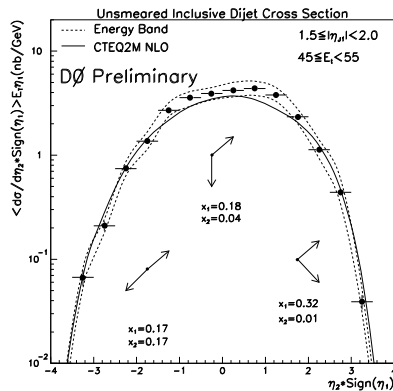


FIG. 63. D0 dijet triple differential cross section vs. the rapidity of the second jet. Data are compared to a QCD calculation using the CTEQ2M parton distribution functions.

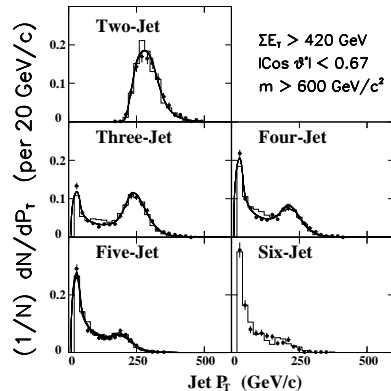


FIG. 64. CDF jet P_T spectra for large E_T events containing 2-6 jets. The data (points) are compared with the NJETS leading-order calculation (curve) and the HERWIG parton-shower program (histogram).

and a parton-shower monte carlo. The former, which does not produce a parton shower, may underestimate low P_T jets. The latter, which begins with a $2 \rightarrow 2$ process at tree level, doesn't describe intermediate P_T jets as well.

4. Jet Shapes

D0 has used a cluster algorithm to investigate the internal structure of jets (39). Figure 65 shows the monte carlo to data ratio of the number of subjets within a jet as a function of the rapidity cutoff in the clustering. The latest version of HERWIG, which produces parton showers with full angular ordering, agrees very well with the data.

To check the kinematic effect of multiple-gluon emission, D0 looked at the jet azimuthal correlation in two-jet events as a function of the rapidity separation between the jets (40). The correlation, which gets weaker as $\Delta\eta$ increases, is well reproduced by a parton shower program with complete angular ordering (Fig. 66).

B. Photon Production

1. Inclusive γ Production

One of the questions from the last $\bar{p}p$ Workshop was the discrepancy between the CDF cross section and theory for photons with P_T below 30 GeV/c. At this meeting, results were presented from both CDF and D0 (41). The D0

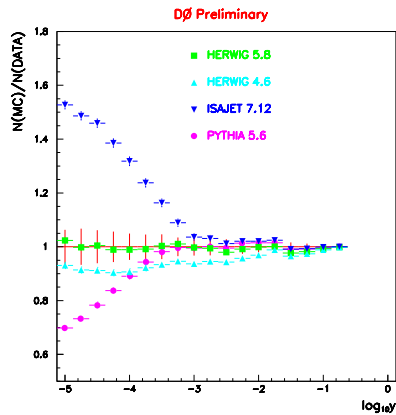


FIG. 65. Monte Carlo to D0 data ratio for the number of subjects found in a jet vs. the rapidity cutoff.

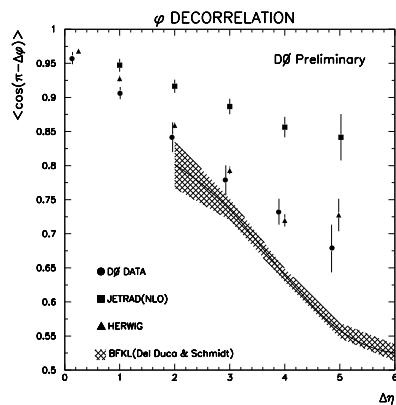


FIG. 66. The D0 mean azimuthal separation of jets as a function of their rapidity separation.

cross section (Fig. 67) agrees with theory for the full P_T range above 10 GeV/c. However their systematic uncertainties are such that they are also consistent with the CDF data. CDF systematic uncertainties are much smaller because photon detection efficiency is calibrated from reconstructed π^0 , η , and ρ^\pm mesons (Figs. 68 and 69). The new data confirm the excess seen in the past. The explanation appears to be the K_T kick provided by initial-state gluon radiation. Figure 70 shows agreement with the data when a parton shower is added to the NLO QCD calculation. Such an effect is also seen in the diphoton cross section described below.

2. $\gamma\gamma$ Production

The CDF production cross section for photon pairs, shown in Fig. 71, agrees within errors with a NLO QCD calculation (42). Since the energies and directions of the photons are well measured, the transverse momentum of the photon pair provides good information on the “ K_T kick”, the P_T produced by initial state gluon radiation. Figure 72 shows the measured $P_T^{\gamma\gamma}$ distribution. The monte carlo calculation that includes parton shower effects describes the data better than a NLO QCD calculation alone.

3. $\gamma + Jet$

The rapidity distribution of jets in inclusive photon events is sensitive to the gluon distribution function in the proton since the dominant production mechanism is $qg \rightarrow \gamma q$ (41). Figure 73 shows that the differences between gluon distributions become quite large for large rapidity jets.

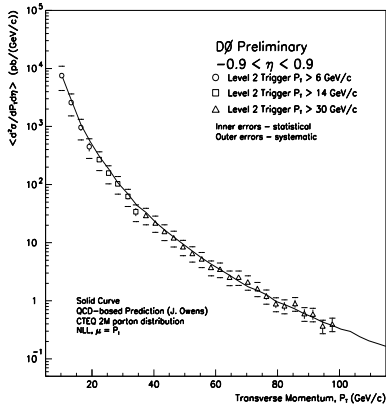


FIG. 67. D0 inclusive γ cross section compared to a NLO QCD calculation.

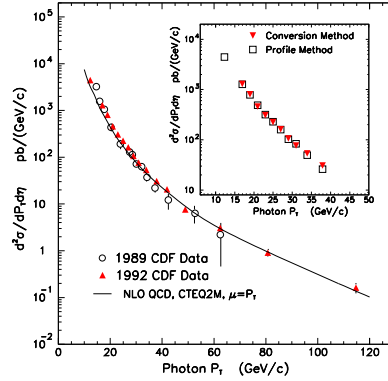


FIG. 68. CDF inclusive γ cross section compared to a NLO QCD calculation.

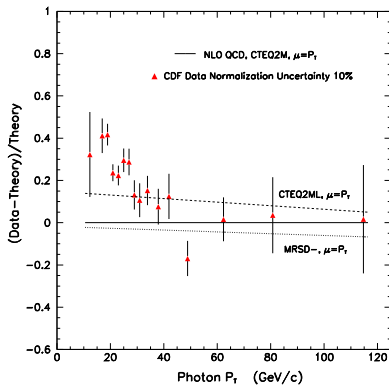


FIG. 69. The difference between the CDF γ cross section and the NLO QCD theory.

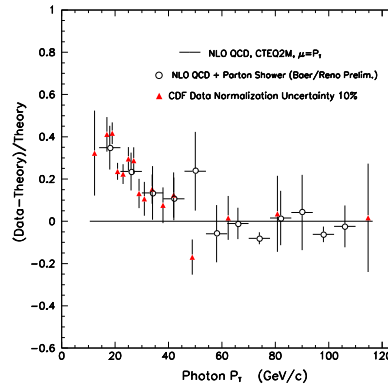


FIG. 70. The difference between the CDF γ cross section and NLO QCD with and without the addition of a parton shower.

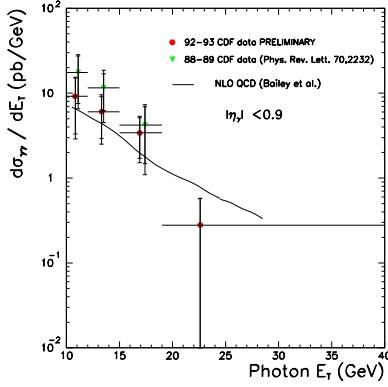


FIG. 71. CDF $\gamma\gamma$ production cross section as a function of γE_T .

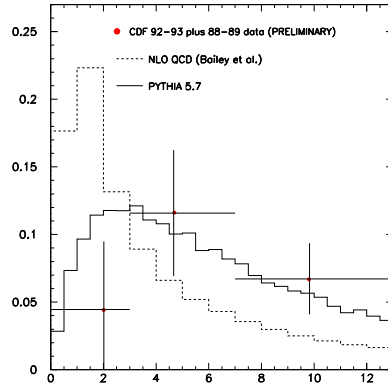


FIG. 72. The $P_T^{\gamma\gamma}$ distribution (in GeV/c) in CDF $\gamma\gamma$ events compared to a NLO QCD calculation and a parton shower monte carlo.

6

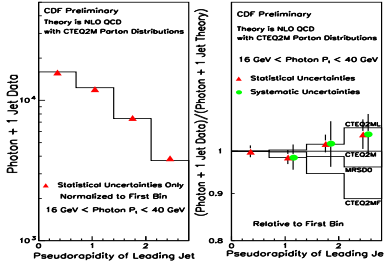


FIG. 73. The CDF $\gamma + \text{jet}$ cross section compared to theory using a number of modern parton distribution functions.

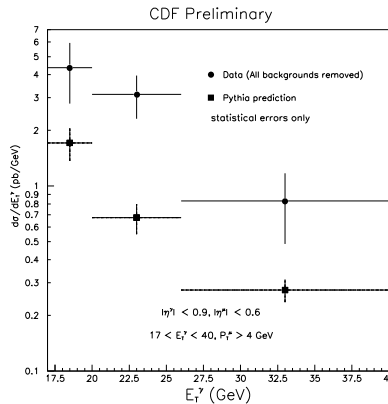


FIG. 74. CDF γ production cross section for events containing a muon.

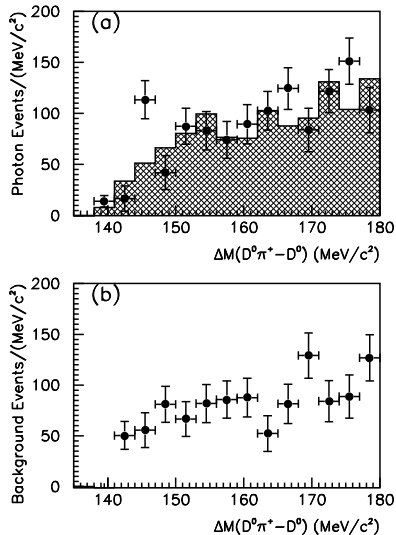


FIG. 75. The $D^0\pi^+ - D^0$ mass difference in (a) CDF γ events and (b) background events. The shaded region is the expected background. The excess near 145 MeV/c² is due to the D^* .

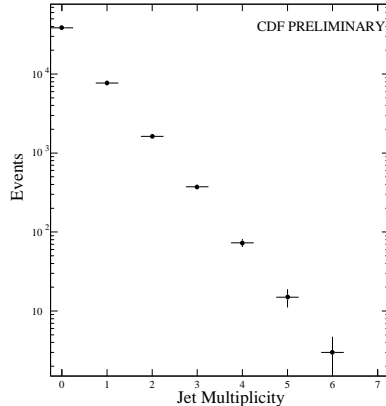


FIG. 76. The jet multiplicity in CDF W events.

4. $\gamma + \text{Charm}$

By detecting a c -quark jet in a large P_T photon event, the process $c\bar{g} \rightarrow \gamma c$ can be isolated. This provides a measurement of the charm distribution function of the proton. CDF employs two techniques to identify c quarks (42). Figure 74 shows the γE_T distribution for events containing a muon. The other method, which requires an identified D^* in addition to the γ (Fig. 75), obtains a production cross section of $0.48 \pm 0.15 \pm 0.07$ nb, to be compared to a theoretical calculation of 0.2 nb. For both techniques, the measured cross section is larger than the theoretical prediction. This of course is true also for other heavy flavor production at Tevatron Collider energies, B production and perhaps even top production.

C. Production of W/Z + Jets

In addition to being an interesting process in its own right, the production of a vector boson with jets is an important background in the study of the top quark and the search for exotic objects. It also represents an important systematic in measuring the W mass.

There are now large W and Z data samples with which to study jet properties (Fig. 76) (43). Many characteristics have been investigated (Figs. 77,

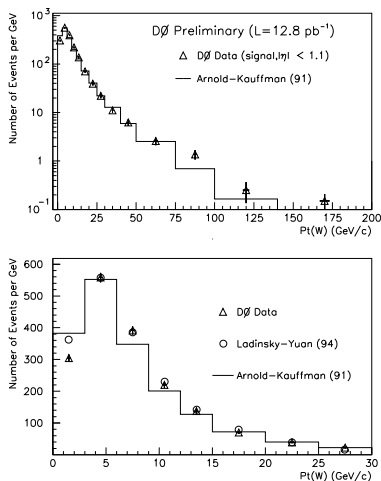


FIG. 77. The W P_T distribution from D0 compared to a NLO calculation.

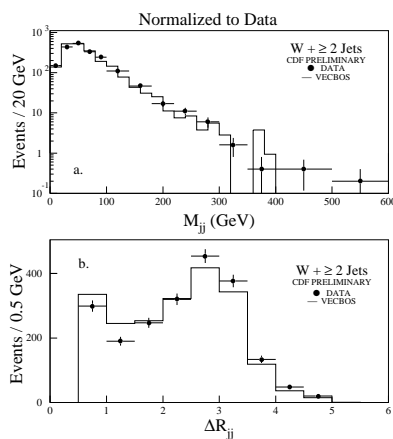


FIG. 78. The (a) dijet invariant mass and (b) jet separation in CDF events with a W and at least 2 jets.

78); the agreement with leading-order and next-to-leading-order calculations is generally good.

D0 used their W event samples with and without jets to measure α_s (44). Figure 79 shows the ratio of the numbers of $W + 1$ -jet to $W + 0$ -jet events compared to theoretical calculations for different values of α_s . In Fig. 80, the measured ratio is compared to theoretical calculations as a function of the assumed α_s . It is interesting to note that the experimental value is higher than all of the calculations. Whether this is merely a statistical fluctuation in the data or a more interesting problem remains to be seen.

D. Rapidity Gaps and Hard Diffraction

If a collision produces two high-momentum objects, and between them is a large rapidity region devoid of particles, that region is a rapidity gap. Such events can be produced just by a statistical fluctuation. However if the two high momentum objects were produced by the exchange of a color-singlet state, rapidity gaps would occur much more often. CDF and D0 have observed rapidity gaps in dijet events (Fig. 81) (45). For jet rapidity separations greater than 2-3 and jet E_T above 20-30 GeV, the excess of rapidity-gap events above that due to statistical fluctuation in normal events is approximately 1.5% of dijet events. This is consistent with estimates that have been made for dijet production through the exchange of a Pomeron.

CDF has also searched for rapidity gaps in events containing a W boson (46). No rapidity gap excess is observed (Fig. 82); this limits the possible hard quark content of the Pomeron. Goulianos has a model of the Pomeron that is consistent with rapidity gap data at both HERA and $\bar{p}p$ colliders.

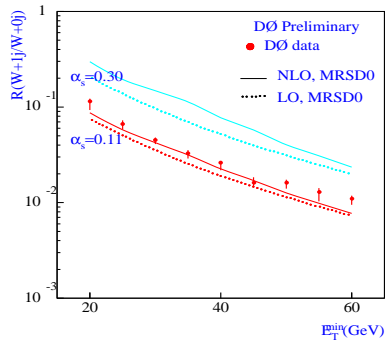


FIG. 79. The ratio of the number of DØ W events with 1-jet to 0-jets as a function of the minimum jet E_T .

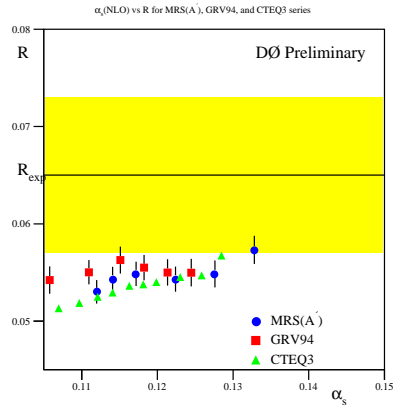


FIG. 80. The ratio of the number of DØ W events with 1-jet to 0-jets compared to theoretical calculations for different assumed values of α_s .

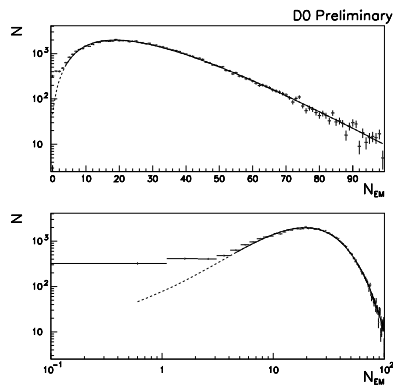


FIG. 81. Number of calorimeter towers with $E > 200$ MeV in the η region between jets, for $\Delta\eta > 3$. The low- N excess above the fit is the rapidity-gap signature.

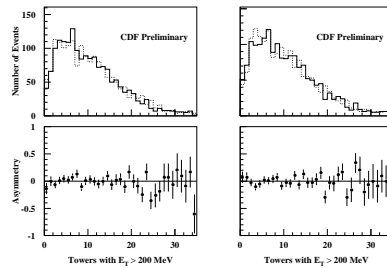


FIG. 82. Charge (left) and angle (right) correlated (solid) and anti-correlated (dashed) multiplicity distributions in the forward region for W events. A positive asymmetry at low multiplicity would indicate rapidity gaps.

VII. CONCLUSIONS

Most of the questions raised at the 9th $\bar{p}p$ Workshop have been answered. QCD does adequately describe γ production below 30 GeV when parton-shower effects are included. The CDF and D0 b -production cross sections are consistent within their quoted uncertainties. So far the Tevatron is living up to its billing as a world-class b -physics facility, but the final assessment awaits more integrated luminosity and detector improvements. It is still unclear how small an uncertainty can be achieved for the W mass, but so far it has decreased as one over the square root of the integrated luminosity. The quest for objects beyond the Minimal Standard Model continues, as always with an eye toward the “zoo events.” The biggest question from the last Workshop has been definitively answered. The top quark is discovered and its mass measured.

But, as always, new questions arise and some old questions remain. Is the jet-production cross section at large P_T adequately described by NLO QCD? Can the detailed distributions in many-jet events be understood? Is the production cross section for a photon plus a charm quark larger than expected? In fact, are all heavy quark production cross sections in high-energy $\bar{p}p$ collisions larger than predicted by NLO QCD calculations? Will the Tevatron live up to its billing as a world-class b -physics facility? How small will $\sigma(M_W)$ get? How small will $\sigma(M_{t_{op}})$ get? Will the study of the $t\bar{t}$ system reveal any new secrets of Nature? And, of course, is there anything beyond the Minimal Standard Model?

The physics opportunities at hadron colliders are enormous, but to reach them there are large experimental challenges to be met. These are being attacked on the accelerator and detector fronts for both the Tevatron and the LHC. In the short term, the goal must be to collect a very large data sample, $\geq 200 \text{ pb}^{-1}$, at the Tevatron. Beyond that, the Main Injector and upgrades to the CDF and D0 detectors should be completed as quickly as possible. In the long term, there should be further upgrades to the Tevatron Collider program in the U.S. and the completion of LHC, Atlas, and CMS in Europe.

The 18 months since the last $\bar{p}p$ Workshop have been an extremely exciting time. The seeds have been sown for many interesting and important studies in the future. If we are extraordinarily fortunate, even more so than we have been so far, perhaps at the next $\bar{p}p$ Workshop we will be discussing an entirely unexpected discovery!

REFERENCES

1. 9th *Topical Workshop on Proton-Antiproton Collider Physics*, edited by K. Kondo and S. Kim (Universal Academy Press, Tokyo, 1994).
2. Jay Hauser, these proceedings.
3. Lee Lueking, these proceedings.
4. Daniel Claes, these proceedings.
5. Amber Boehnlein, these proceedings.

6. Seongwan Park, these proceedings.
7. Robert Harris, these proceedings.
8. Kamel Bazizi, these proceedings.
9. Pat Lukens, these proceedings.
10. Sandor Feher, these proceedings.
11. Gerry Bauer, these proceedings.
12. E. Braaten and S. Fleming, Phys. Rev. Lett **74**, 3327 (1995).
13. Michelangelo Mangano, these proceedings.
14. Franco Bedeschi, these proceedings.
15. J. Bartelt *et al*, Phys. Rev. Lett **71**, 1680 (1993).
16. Jonathan Rosner, these proceedings.
17. F. Abe *et al*, Phys. Rev. **D50**, 2966 (1994); Phys. Rev. Lett **73**, 225 (1994).
18. F. Abe *et al*, Phys. Rev. Lett **74**, 2626 (1995).
19. S. Abachi *et al*, Phys. Rev. Lett **74**, 2632 (1995).
20. Robert Roser, these proceedings.
21. Joseph Incandela, these proceedings.
22. Steven Vajcik, these proceedings.
23. Jeffrey Bantly, these proceedings.
24. Pushpalatha Bhat, these proceedings.
25. Mark Strovink, these proceedings.
26. Morris Binkley, these proceedings.
27. E. Berger and H. Contopanagos, Argonne preprint ANL-HEP-PR-95-31.
28. Dorothee Schaile, these proceedings.
29. Anthony Spadafora, these proceedings.
30. F. Abe *et al*, Phys. Rev. Lett **74**, 341 (1995).
31. Pawel de Barbaro, these proceedings.
32. Young-Kee Kim, these proceedings.
33. Douglas Benjamin, these proceedings.
34. Thomas Diehl, these proceedings.
35. Walter Giele, these proceedings.
36. Anwar Bhatti, these proceedings.
37. Freedy Nang, these proceedings.
38. Steve Geer, these proceedings.
39. Richard Astur, these proceedings.
40. Nikos Varelas, these proceedings.
41. Jodi Lamoureux, these proceedings.
42. Robert Blair, these proceedings.
43. Danilo Puseljic, these proceedings.
44. Jaehoon Yu, these proceedings.
45. Iain Bertram, these proceedings.
46. Dino Goulianos, these proceedings.